

Creation and annihilation of artificial magnetic skyrmions with the electric field

Jun Cheng(程军), Liang Sun(孙亮), Yike Zhang(张一可), Tongzhou Ji(吉同舟), Rongxing Cao(曹荣幸), Bingfeng Miao(缪冰锋), Yonggang Zhao(赵永刚), and Haifeng Ding(丁海峰)
Citation: Chin. Phys. B, 2024, 33 (**3**): 037501. DOI: 10.1088/1674-1056/ad188f
Journal homepage: http://cpb.iphy.ac.cn; http://iopscience.iop.org/cpb

What follows is a list of articles you may be interested in

Oscillation of Dzyaloshinskii-Moriya interaction driven by weak electric fields

Runze Chen(陈润泽), Anni Cao(曹安妮), Xinran Wang(王馨苒), Yang Liu(柳洋), Hongxin Yang(杨洪新), and Weisheng Zhao(赵巍胜)
Chin. Phys. B, 2024, 33 (**2**): 027501. DOI: 10.1088/1674-1056/ad0f85

Room-temperature creation and manipulation of skyrmions in MgO/FeNiB/Mo multilayers

Wen-Hui Liang(梁文会), Jian Su(苏鉴), Yu-Tong Wang(王雨桐), Ying Zhang(张颖), Feng-Xia Hu(胡凤霞), and Jian-Wang Cai(蔡建旺)
Chin. Phys. B, 2023, 32 (**12**): 127504. DOI: 10.1088/1674-1056/acf5d4

In-plane spin excitation of skyrmion bags

Shuang Li(李爽), Ke-Xin Li(李可欣), Zhao-Hua Liu(刘照华), Qi-Yuan Zhu(朱起源), Chen-Bo Zhao(赵晨博), Hu Zhang(张虎), Xing-Qiang Shi(石兴强), Jiang-Long Wang(王江龙), Rui-Ning Wang(王瑞宁), Ru-Qian Lian(连如乾), Peng-Lai Gong(巩朋来), and Chen-Dong Jin(金晨东)
Chin. Phys. B, 2023, 32 (**11**): 117503. DOI: 10.1088/1674-1056/acd327

Gate-voltage control of alternating-current-driven skyrmion propagation in ferromagnetic nanotrack devices

Xin-Yi Cai(蔡心怡), Zhi-Hua Chen(陈志华), Hang-Xiao Yang(杨航霄), Xin-Yan He(何鑫岩), Zhen-Zhen Chen(陈珍珍), Ming-Min Zhu(朱明敏), Yang Qiu(邱阳), Guo-Liang Yu(郁国良), and Hao-Miao Zhou(周浩淼)
Chin. Phys. B, 2023, 32 (**6**): 067502. DOI: 10.1088/1674-1056/acb420

Magnetic triangular bubble lattices in bismuth-doped yttrium iron garnet

Tao Lin(蔺涛), Chengxiang Wang(王承祥), Zhiyong Qiu(邱志勇), Chao Chen(陈超), Tao Xing(邢弢), Lu Sun(孙璐), Jianhui Liang(梁建辉), Yizheng Wu(吴义政), Zhong Shi(时钟), and Na Lei(雷娜)
Chin. Phys. B, 2023, 32 (**2**): 027505. DOI: 10.1088/1674-1056/aca604

RAPID COMMUNICATION

Creation and annihilation of artificial magnetic skyrmions with the electric field

Jun Cheng(程军)[1,†], Liang Sun(孙亮)[1,2,†], Yike Zhang(张一可)[3,4], Tongzhou Ji(吉同舟)[1], Rongxing Cao(曹荣幸)[5], Bingfeng Miao(缪冰锋)[1,2,‡], Yonggang Zhao(赵永刚)[3,4,§], and Haifeng Ding(丁海峰)[1,2,¶]

[1] *National Laboratory of Solid State Microstructures and Department of Physics, Nanjing University, Nanjing* 210093, *China*
[2] *Collaborative Innovation Center of Advanced Microstructures, Nanjing University, Nanjing* 210093, *China*
[3] *Department of Physics, State Key Laboratory of Low-Dimensional Quantum Physics, Tsinghua University, Beijing* 100084, *China*
[4] *Frontier Science Center for Quantum Information, Tsinghua University, Beijing* 100084, *China*
[5] *College of Electrical, Energy and Power Engineering, Yangzhou University, Yangzhou* 225127, *China*

(Received 19 October 2023; revised manuscript received 14 December 2023; accepted manuscript online 25 December 2023)

Recent theory and experiments show that artificial magnetic skyrmions can be stabilized at room temperature without the need for the external magnetic field, casting strong potentials for the device applications. In this work, we study the electric field manipulation of artificial magnetic skyrmions imprinted by Co disks on CoPt multilayers utilizing the micromagnetic simulations. We find that the reversible annihilation and creation of skyrmions can be realized with the electric field via the strain mediated magnetoelastic coupling. In addition, we also demonstrate controllable manipulation of individual skyrmion, which opens a new platform for constructing magnetic field-free and low-energy dissipation skyrmion based media.

Keywords: skyrmions, magnetic anisotropy, micromagnetic simulations

PACS: 75.30.Gw, 75.78.Cd, 12.39.Dc **DOI:** 10.1088/1674-1056/ad188f

1. Introduction

Magnetic skyrmions are topologically protected chiral spin textures.[1,2] They possess particle-like feature with nanoscale size and can be driven with ultralow-density current, exhibiting great potential for applications in information storage and logic devices.[3–9] Magnetic skyrmions can be stabilized by the bulk Dzyaloshinskii–Moriya interaction (DMI) in inversion symmetry broken materials[10–15] as well as by the interfacial DMI in normal metal/ferromagnet (NM/FM) heterostructures.[16–18] Besides, artificial magnetic skyrmion crystals have been proposed and experimentally demonstrated in Co nano disks decorated perpendicularly magnetization Ni films, Co/Pt and Co/Pd multilayers at room temperature under zero external field.[19–23] Artificial skyrmion is stabilized by the competition between the exchange energy, dipolar energy and anisotropy energy, which does not necessarily involve any DMI. Thus, it significantly widens the scope of material selections for fundamental research and practical applications. In addition, artificial skyrmion crystal has controllable topological number and similar dynamic features as the DMI-induced skyrmion crystal.[24]

Controllable creation and annihilation of skyrmion are the prerequisites for the skyrmion-based applications. Extensive efforts have been paid to the utilization of the spin-polarized current.[17,25–30] The required high-density current, however, will result in significant power consumption and instability of skyrmions due to the rise of device temperature. Alternatively, electric-field-controlled magnetism provides an energy-efficient approach to manipulate skyrmion without Joule heating.[31–36] The hybrid FM and ferroelectric (FE) heterostructures have been demonstrated to realize large electric-field-controlled magnetism at room temperature,[37–40] where the magneto-electric (ME) coupling is mediated by strain. The ME coupling was also theoretically proposed and experimentally demonstrated to control the DMI induced magnetic skyrmions.[41–44] As an important member of the magnetic skyrmion family, the study of the electric-field induced nucleation and annihilation of artificial skyrmion are, however, still missing.

In this work, we study the electrical manipulation of the artificial magnetic skyrmions through micromagnetic simulations. The skyrmions are composed of nano-sized Co disk array patterned onto Pt/Co multilayers with perpendicular magnetic anisotropy (PMA). And the whole heterostructure lies on an FE substrate, wherein the PMA of the CoPt film can be modulated by the electric field through strain. Our simulations clearly demonstrate the reversible annihilation and creation of skyrmions without the DMI and magnetic field. Moreover, benefiting from the local application of the electric field, con-

[†]These authors contributed equally to this work.
[‡]Corresponding author. E-mail: bfmiao@nju.edu.cn
[§]Corresponding author. E-mail: ygzhao@tsinghua.edu.cn
[¶]Corresponding author. E-mail: hfding@nju.edu.cn

© 2024 Chinese Physical Society and IOP Publishing Ltd

trollable manipulation of individual skyrmion in CoPt film can be realized and specific skyrmion patterns form. These results provide a new direction for developing skyrmion-based information storage and computing technology.

2. Results and discussion

The schematic diagram of the concept of the annihilation and creation of artificial skyrmions with the electric field is presented in Fig. 1. An array of magnetic disks is patterned onto the continuous film with PMA (blue layer) [Fig. 1(a)], which lies on a piezoelectric substrate (dark gray layer). The PMA film acts as the top gate, while an additional metallic film, such as a gold layer beneath the piezoelectric substrate serves as the bottom gate. With the suitable height and diameter, the ground state of the magnetic disks is the vortex state. The edge-clipped geometry is further used to break the circular symmetry of the vortex, so that both the circulation and polarity of the vortex can be aligned uniformly with suitable magnetic field operation.[19,45,46] Due to the interfacial exchange coupling, the magnetic disks would imprint the vortex structures into the underlying PMA layer. As long as the magnetization of the PMA layer surrounding the magnetic disks is opposite to the imprinted vortex polarity, a magnetic skyrmion lattice is formed [Fig. 1(b)]. After applying an electric field across the piezoelectric substrate, the strain of substrate in combination with the magnetoelastic effect in PMA layer results in a modulation of the PMA. For simplicity, we assume a linear relation between the PMA constant and the electric field as $K_\perp(E) = \alpha|E| + K_\perp(0)$, where $\alpha > 0$ is a constant denoting the strength of the converse magneto-electric effect. Note here we only consider the common symmetric strain response with the electric field. When an asymmetric response, especially with nonzero remanence as reported in Ref. [44] is used, such a characteristic may also have the potential for non-volatile control of the magnetic skyrmion. With increasing electric field, the enhanced PMA strength would shrink the size of the imprinted vortex core. Above a critical value, the skyrmion structure in PMA layer is no longer stable and evolves into the perpendicular state. This process corresponds to the annihilation of skyrmions, as shown in Fig. 1(c). Conversely, the PMA value of the PMA layer decreases when weakening the electric field. Due to the exchange coupling between PMA layer and the vortex structure in the patterned magnetic disks, chiral magnetic structure in the PMA layer would emerge again, leading to the reemergence of the skyrmion [Fig. 1(d)]. Therefore, the annihilation and creation of skyrmions can be achieved by changing the anisotropy constant of the film with PMA through the electric field only. Both the annihilation and creation processes are reversible, magnetic field-free, and energy-efficient since only the voltage pulses are applied.

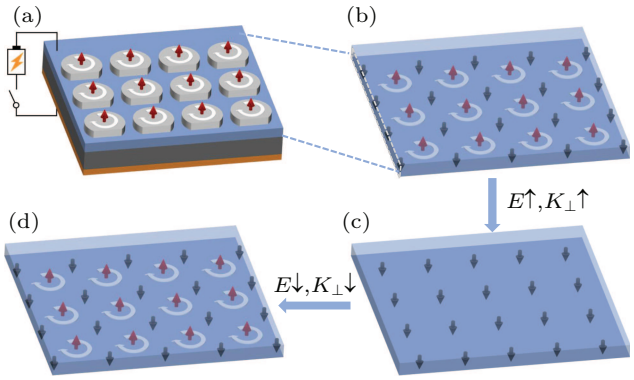


Fig. 1. Proposed pathway for the annihilation and creation of skyrmions with the electric field. (a) Magnetic disks arranged on top of the magnetic film with perpendicular anisotropy. The electric field is applied between the film and the bottom electrode of the substrate, the arrow indicates the orientation of the local magnetic moments. (b) The perpendicularly magnetized film with vortex magnetic moments imprinted by the magnetic disks. After being applied an increasing (decreasing) electric field E, the perpendicular anisotropy constant $K_\perp$ will enhance (reduce), leading to (c) the annihilation and (d) the creation of skyrmions, respectively.

In the following, we will demonstrate our proposal with micromagnetic simulations utilizing the OOMMF code.[47] Co and CoPt multilayer are selected as the materials of magnetic disks and PMA layer, respectively. The material parameters used in simulations are[19] the exchange constants of $A^{\mathrm{Co}} = 2.5\times10^{-11}$ J/m, $A^{\mathrm{CoPt}} = 1.5\times10^{-11}$ J/m, the saturation magnetization of $M^{\mathrm{Co}} = 1.4\times10^{6}$ A/m, $M^{\mathrm{CoPt}} = 5.0\times10^{5}$ A/m, and the uniaxial perpendicular magnetic anisotropy for the CoPt films is $K_\perp = 3.0\times10^{5}$ J/m^3 in the absence of the electric field. We assume the interlayer exchange constant between the Co disk and CoPt film to be $A^{\mathrm{Co-CoPt}} = 2.0\times10^{-12}$ J/m, which can be modulated by adding non-magnetic insertion layer. The Co disks with diameter $D = 120$ nm and thickness $t_{\mathrm{Co}} = 18$ nm are arranged in a square lattice. The spacing between the center of the Co disks S is 180 nm. And the CoPt film thickness t_{CoPt} is 8 nm. In the simulations, we use a two-dimensional periodical boundary condition within the film plane, and a grid size of $2\times2\times1$ nm^3. For simplicity, we assume that the strain only acts uniformly on the CoPt films and has no apparent influence on the top Co disks. As the typical magnetic field required to switch the polarity of the magnetic vortex is ~ 500 mT,[21] the weak magnetoelastic effect of the in-plane Co disk is expected to have little influence on the vortex structure.[48]

We first apply a perpendicular magnetic field (800 mT, along the z-direction) to configure the polarity of the Co disks. Meanwhile, an in-plane magnetic field (300 mT) pulse along the cutting edge of the Co disks is applied to align their circulation. After releasing the magnetic field, all the disks are in the vortex configuration with the same polarity and circulation. Due to the coupling between the Co and CoPt layer, the vortices also emerge in the PMA–CoPt layer. Lastly, an opposite

perpendicular magnetic field (−200 mT, a value in between the switching fields of CoPt layer and the vortex polarity) is applied to switch the magnetization of the CoPt layer surrounding the vortex structures, while leaving the polarity of vortices unaffected. After these magnetic field operations,[19,21] a uniform magnetic skyrmion lattice is stabilized as shown in Fig. 2(a). And the inset presents the distribution of local magnetic moments of the above Co disks. Figures 2(b)–2(d) show the evolution of skyrmion with increasing PMA constant. From $K_\perp = 3.0\times10^5$ J/m^3 to $K_\perp = 8.0\times10^5$ J/m^3, the size of the skyrmion core (defined as the central area of the skyrmion within the line $m_z = 0$) shrinks. When $K_\perp > 7.5\times10^5$ J/m^3, the skyrmion core in the CoPt layer vanishes and the skyrmion disappears. Namely, the whole CoPt layer almost enters a uniform perpendicular state with only small in-plane magnetization component beneath the Co disks. We note that the vortex structures persist in the capping Co disks due to the relatively weak coupling between Co and Co/Pt. Conversely, we can also create skyrmions by decreasing the PMA of the CoPt film. As demonstrated in Figs. 2(e)–2(g), more in-plane magnetization component develops beneath the Co disks with decreasing PMA value and eventually transforms into the vortex state (below 2.8×10^5 J/m^3). Due to the coupling between Co and CoPt, the vortex cores in these two materials are of the same polarity. Therefore, the skyrmion structures are nucleated without applying any magnetic field. By further reducing the anisotropy constant, the diameter of the skyrmion is slightly enhanced to lower the Zeeman energy [Fig. 2(h)].

Figure 3(a) summarizes the evolution of the calculated skyrmion number per unit cell with the change of the magnetic anisotropy constant $K_\perp$. It shows a loop changing between two discrete numbers of "1" and "0", evidencing the sweeping between two topological states. We have herein achieved reversible annihilation and creation of skyrmions by changing the PMA constant of the CoPt film through micromagnetic simulation. And the required variation of PMA constant from annihilation to recreation is around 63%. We note that such amount of change of PMA constant has been demonstrated experimentally,[44] indicating the feasibility of the electric field modulation of artificial skyrmion at room temperature. Furthermore, the magnetoelastic coupling coefficient for (111)-textured Co/Pt is up to 2.38×10^{-2} J/(m$^2\cdot$V) at room temperature in literature.[49] Therefore, we can estimate the needed electric field E which is 19.7 MV/m for our calculated CoPt system. It has been reported that high-quality single crystal PMN-PT films can be grown on silicon substrate, which is compatible with semiconductor industry.[50] If a μm-thickness piezoelectric film is used, the required voltage is about 20 V. We would like to mention that the magnetic anisotropy of the Co/Pt perpendicular film can also be regulated by the voltage controlled magnetism anisotropy (VCMA) method, the equivalent magnetic anisotropy changes are about 10^6–10^7 J/m^3 [51–53] with applying a few Volts. The reported range is more than we need, showing the feasibility of our proposed method. It is worth noting that we have mainly considered the influence of perpendicular anisotropic changes here. In real samples, the electric field may also cause other changes such as the exchange constant, Dzyaloshinskii–Moriya interaction, etc.[44] The combined effect of multiple factors may further reduce the required changes of PMA.

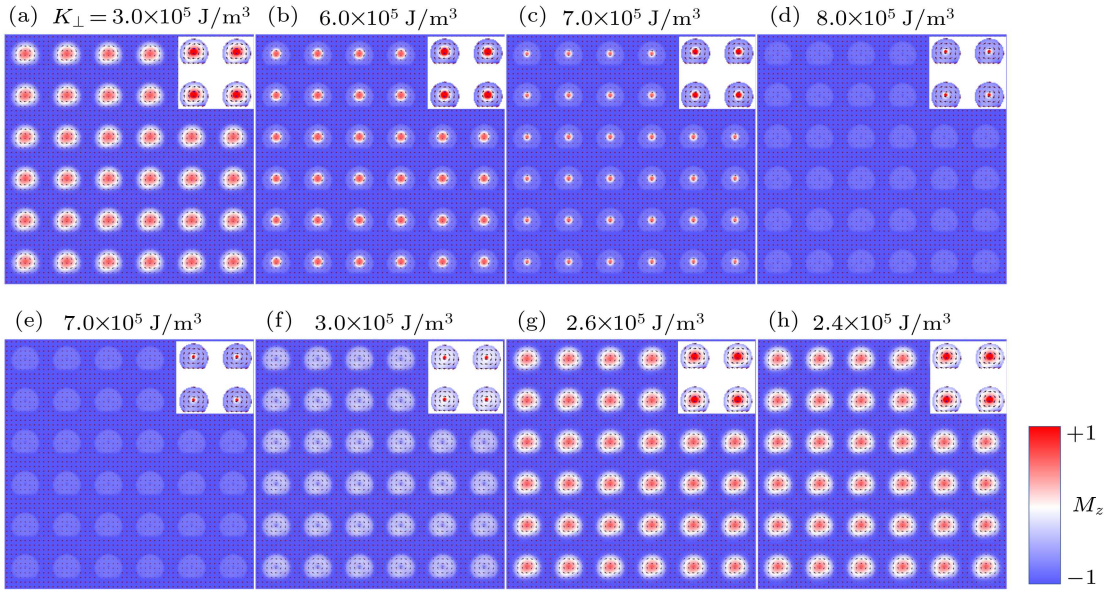


Fig. 2. The annihilation and creation of skyrmions with increasing/decreasing PMA. (a) Top view of magnetic moment distribution of CoPt film with $K_\perp = 3.0\times10^5$ J/m^3, the inset represents the situation of Co disks. With the increase of $K_\perp$, the diameter of skyrmions decreases until it disappears, shown in (b)–(d). In turn, when decreasing the magnitude of $K_\perp$, skyrmions are created after the critical value is reached, as shown in (e)–(h). The color bar represents the projection of local moments along the z-direction, $+1/-1$ indicates that the magnetization is saturated along the $+z/-z$ direction, respectively.

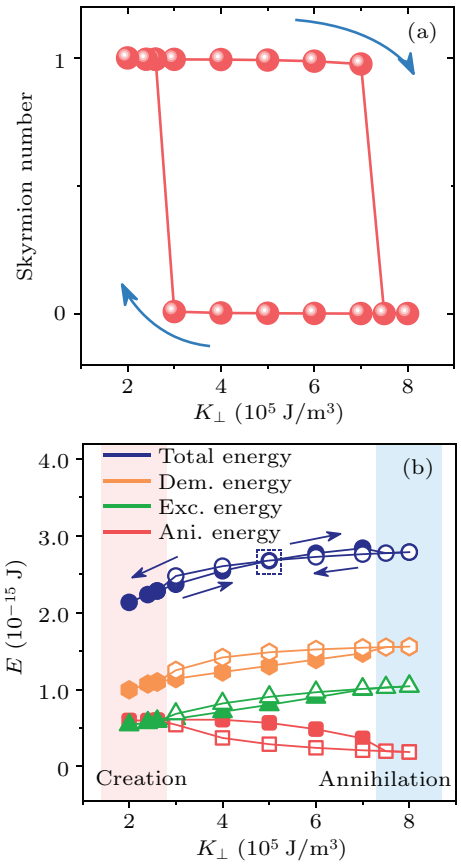


Fig. 3. The evolution of skyrmion number and magnetic energy terms (the total energy, uniaxial anisotropy energy, exchange energy, demagnetization energy) with different anisotropy constants. (a) Skyrmion numbers "1" and "0" represent skyrmion state and non-skyrmion state, respectively. (b) The blue (pink) shadow area represents the regions for the annihilation (creation) of skyrmions, respectively. The solid (open) symbols represent the skyrmion (non-skyrmion) state. The blue arrows indicate the sweeping direction, and the dashed square indicates the case both the skyrmion and non-skyrmion states have the same energy.

To gain a deeper understanding of the skyrmion's annihilation and creation behavior, we conduct further analysis. We perform calculations with different Co disks spacing S. The simulations show that when S decreases from 180 nm to 130 nm, the $K_\perp$ for skyrmion annihilation remains almost unchanged while $K_\perp$ for the skyrmion nucleation changes from 2.8×10^5 J/m^3 to 2.6×10^5 J/m^3, suggesting weak influence of the dipolar interaction between the disks. For simplicity, the exchange constant A^{CoPt} is assumed to be uniform across the CoPt films in our simulation. Besides, we also perform simulations with different A^{CoPt} values for the in-plane and vertical direction, such as the A^{CoPt} values on vertical direction are decreased (increased) to 1.0×10^{-11} J/m (2.25×10^{-11} J/m) respectively while keeping the in-plane A^{CoPt} unchanged. The simulations show that, in both cases, the changes of A^{CoPt} only have minor influence on the critical value $K_\perp$ for skyrmions annihilation and creation.

Figure 3(b) presents the evolution of the total energy E_{tot} as well as the corresponding demagnetization energy E_{dem}, anisotropy energy E_{ani} and exchange energy terms E_{exc} during the process of annihilation and creation (corresponding to the process in Fig. 2). According to the evolution of the total energy E_{tot} with the variation of $K_\perp$, the stability diagram can be defined as three regions. At low $K_\perp$ (pink area), the magnetic structure has only one stable state, namely the skyrmion state (solid symbols). At high $K_\perp$ (light blue area), the magnetic structure has only one stable state, namely, the non-skyrmion state (open symbols). In the middle region (white area), both the skyrmion and non-skyrmion states are stable but with one as the metastable state. This is further supported by the evolution of E_{dem}, E_{ani} and E_{exc}, which show hysteresis loop like behavior. With increasing $K_\perp$, both E_{dem} and E_{exc} increase but E_{ani} decreases. The competition between them results in an interesting evolution of the E_{tot} in this region. At $K_\perp\approx5\times10^5$ J/m^3, both states have almost the same total energy (marked by the dashed square). Namely, the metastable and stable states swap their statuses at $K_\perp\approx5\times10^5$ J/m^3. When $K_\perp$ deviates more from this value, the total energy difference between these two states becomes larger. And the metastable state becomes unstable, resulting in a change of magnetic configuration, either from non-skyrmion state to skyrmion state or vice versa.

We further study the phase diagram where the skyrmion can be reversibly annihilated and created with different PMA constant $K_\perp$ of the CoPt layer and the exchange constant $A^{\mathrm{Co-CoPt}}$ between Co and Co/Pt. Figure 4(a) presents the result for $D=120$ nm and $S=180$ nm. Within the most region (solid square), the skyrmion structure can be reversibly annihilated and created. And the system can bear stronger perpendicular anisotropy when the interlayer exchange interaction is larger. This can be understood as the skyrmion structures are the results of competition among different energy terms. When the system has large $K_\perp$ and small $A^{\mathrm{Co-CoPt}}$, skyrmion cannot be generated (cross). The CoPt layer beneath the Co disk is dominated by the perpendicular magnetization but with small in-plane curling component. Figure 4(b) presents the case for $D=80$ nm and $S=100$ nm, with all other parameters identical to Fig. 4(a). Due to the decrease of the stability of the skyrmion structure with the decreased size, the region where both annihilation and creation can be achieved becomes much smaller. And for the open square, the skyrmion can only be annihilated but not be recreated. This could be due to the fact that as the diameters of the Co disks further decrease, the energy that they could provide also decreases. And at a certain level, it could not overcome the energy threshold required to induce the recreation of skyrmions. In addition, we also calculate the case with different Co disk and CoPt film thicknesses, the annihilation and recreation of skyrmion state can also be achieved under suitable conditions. The above results show that the manipulations of patterned artificial skyrmions are feasible under various situations.

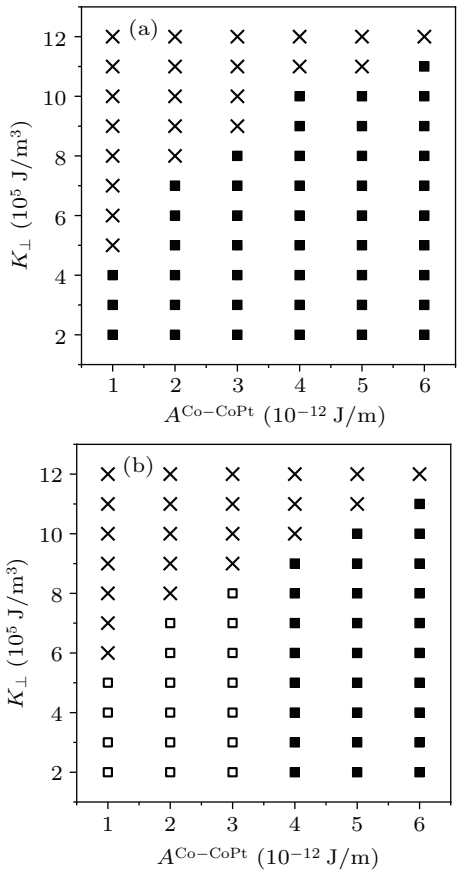


Fig. 4. The phase diagram of skyrmions regions for system with (a) $D = 120$ nm, $S = 180$ nm, and (b) $D = 80$ nm, $S = 100$ nm. $K_\perp$ and $A^{\mathrm{Co-CoPt}}$ are the perpendicular anisotropy constant of CoPt film and the interfacial exchange constant between Co and CoPt, respectively. The solid symbols show skyrmions can be annihilated and created reversibly; the open symbols show skyrmions can only be annihilated, but not be recreated; the cross point shows the skyrmions cannot be generated.

For applications such as the magnetic storage, not only the collective and reversible control of the annihilation and creation of the skyrmion lattice but also the independent manipulation of the individual skyrmion is important. We further demonstrate the local control of individual skyrmion with the electric field. Figure 5(a) presents the studied system with 36 skyrmions in the CoPt layer, where $K_\perp = 2.6 \times 10^5$ J/m^3 and other parameters the same as those used in Fig. 2. For each unit, Co/Pt film is in a square shape and the Co disk locates in the center of the square. The PMA of the CoPt film in the square can be changed by the local strain. Besides, the starting condition of the system is a random distribution of magnetic moments, then the field sequence described in the text above is performed to formulate a uniform magnetic skyrmion lattice [shown in Fig. 5(a)]. Figures 5(b)–5(d) are sequentially obtained by individually changing $K_\perp$ of the underlayer CoPt films of the selected unit cells with Fig. 5(a) as the starting state and without applying any magnetic field. After applying local electric field upon specific 24 unit cells, the PMA constant $K_\perp$ therein increases to 8.0×10^5 J/m^3, while the other 12 unit cells remain unchanged. Our calculations show that the spin configuration transforms from full skyrmions state to "S", "K" and "X" shaped skyrmions patterns [Figs. 5(b)–5(d)], depending on the positions of the local electric field. Therefore, we achieve the encoding of information with a single skyrmion as the unit cell. We note that although the control of number of skyrmions in the skyrmion clusters in a one-by-one manner through an electric field has been reported previously, the authors therein still need assisting magnetic field.[54] In contrast, we herein report the annihilation and creation of individual skyrmions by modulating the PMA constant with the electric field only, which is more energy-efficient. For simplicity, the control of a single unit is performed with a voltage controlled local strain modification only. The strain may have lateral spread. The lateral spread is expected to have a decay away from the unit being controlled. From our simulation shown in Fig. 3(a), the skyrmion annihilation and creation show a square loop with a relatively wide region. This indicates that it requires a large change of strain to modify the configuration. The attenuated strain at the adjacent units thus has no strong influence on their magnetic configurations.

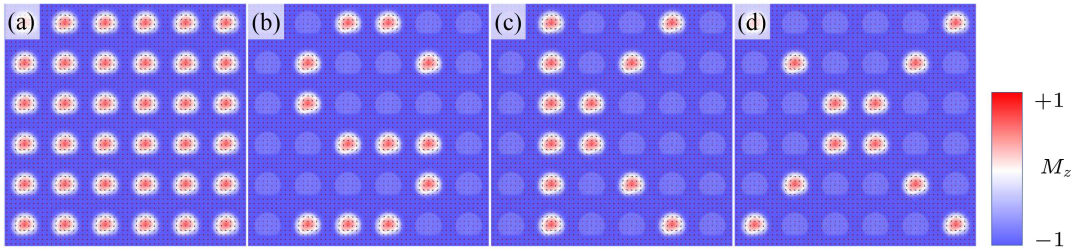


Fig. 5. The schematic of independent control of individual skyrmion with the local electric field applied at different positions. (a) The top view of skyrmions with $K_\perp = 2.6 \times 10^5$ J/m^3. Varying the anisotropy constant of each cell transforms between $K_\perp = 2.6 \times 10^5$ J/m^3 and $K_\perp = 8.0 \times 10^5$ J/m^3, we have achieved the desired "S", "K", "X" shaped skyrmion patterns, as shown from (b) to (d). The color bar represents the projection of local moments along the z-direction, $+1/-1$ indicates that the magnetization is saturated along the $+z/-z$ direction, respectively.

3. Conclusion

In summary, we provide a new pathway to realize the reversible annihilation and creation of artificial magnetic skyrmions in patterned Co disk–Co/Pt multilayer heterostructures through changing the perpendicular anisotropy constant of the CoPt film deposited on piezoelectric substrate with the electric field. In particular, this can be achieved without the need of DMI and magnetic field. A phase diagram is provided which shows that the reversible annihilation–creation behavior can exist over a wide parameters space. Further we

also demonstrate the controllable manipulation of individual skyrmion, providing a new platform for encoding information in skyrmion based media.

Data availability statement

The data that support the findings of this study are openly available in Science Data Bank at https://doi.org/10.57760/sciencedb.j00113.00195.

Acknowledgements

Project supported by the National Key R&D Program of China (Grant Nos. 2021YFB3502400 and 2022YFA1403601), the National Natural Science Foundation of China (Grant Nos. 12274204, 12274203, 51831005, 52172270, 11974165, 92165103, 51971110, 12004329, and 12241402).

References

[1] Skyrme T H R 1961 *Proc. R. Soc. London Ser. A* **262** 237
[2] Skyrme T H R 1962 *Nucl. Phy.* **31** 556
[3] Jonietz F, Mühlbauer S, Pfleiderer C, Neubauer A, Münzer W, Bauer A, Adams T, Georgii R, Böni P, Duine R A, Everschor K, Garst M and Rosch A 2010 *Science* **330** 1648
[4] Fert A, Cros V and Sampaio J 2013 *Nat. Nanotechnol.* **8** 152
[5] Wiesendanger R 2016 *Nat. Rev. Mater.* **1** 16044
[6] Zhou Y 2019 *Natl Sci. Rev.* **6** 210
[7] Yu X Z, Kanazawa N, Zhang W Z, Nagai T, Hara T, Kimoto K, Matsui Y, Onose Y and Tokura Y 2012 *Nat. Commun.* **3** 988
[8] Zhang X, Zhou Y, Ezawa M, Zhao G P and Zhao W 2015 *Sci. Rep.* **5** 11369
[9] Lin S Z, Reichhardt C and Saxena A 2013 *Appl. Phys. Lett.* **102** 222405
[10] Rößler U K, Bogdanov A N and Pfleiderer C 2006 *Nature* **442** 797
[11] Mühlbauer S, Binz B, Jonietz F, Pfleiderer C, Rosch A, Neubauer A, Georgii R and Böni P 2009 *Science* **323** 915
[12] Münzer W, Neubauer A, Adams T, Mühlbauer S, Franz C, Jonietz F, Georgii R, Böni P, Pedersen B, Schmidt M, Rosch A and Pfleiderer C 2010 *Phys. Rev. B* **81** 041203
[13] Yu X Z, Kanazawa N, Onose Y, Kimoto K, Zhang W Z, Ishiwata S, Matsui Y and Tokura Y 2011 *Nat. Mater.* **10** 106
[14] Huang S X and Chien C L 2012 *Phys. Rev. Lett.* **108** 267201
[15] Li Y, Kanazawa N, Yu X Z, Tsukazaki A, Kawasaki M, Ichikawa M, Jin X F, Kagawa F and Tokura Y 2013 *Phys. Rev. Lett.* **110** 117202
[16] Tokunaga Y, Yu X Z, White J S, Rønnow H M, Morikawa D, Taguchi Y and Tokura Y 2015 *Nat. Commun.* **6** 7638
[17] Jiang W, Upadhyaya P, Zhang W, Yu G, Jungfleisch M B, Fradin F Y, Pearson J E, Tserkovnyak Y, Wang K L, Heinonen O, te Velthuis S G E and Hoffmann A 2015 *Science* **349** 283
[18] Chen G, Mascaraque A, N'Diaye A T and Schmid A K 2015 *Appl. Phys. Lett.* **106** 242404
[19] Sun L, Cao R X, Miao B F, Feng Z, You B, Wu D, Zhang W, Hu A and Ding H F 2013 *Phys. Rev. Lett.* **110** 167201
[20] Dai Y Y, Wang H, Tao P, Yang T, Ren W J and Zhang Z D 2013 *Phys. Rev. B* **88** 054403
[21] Miao B F, Sun L, Wu Y W, Tao X D, Xiong X, Wen Y, Cao R X, Wang P, Wu D, Zhan Q F, You B, Du J, Li R W and Ding H F 2014 *Phys. Rev. B* **90** 174411
[22] Li J, Tan A, Moon K W, Doran A, Marcus M A, Young A T, Arenholz E, Ma S, Yang R F, Hwang C and Qiu Z Q 2014 *Nat. Commun.* **5** 4704
[23] Gilbert D A, Maranville B B, Balk A L, Kirby B J, Fischer P, Pierce D T, Unguris J, Borchers J A and Liu K 2015 *Nat. Commun.* **6** 8462
[24] Miao B F, Wen Y, Yan M, Sun L, Cao R X, Wu D, You B, Jiang Z S and Ding H F 2015 *Appl. Phys. Lett.* **107** 222402
[25] Woo S, Litzius K, Krüger B, Im M-Y, Caretta L, Richter K, Mann M, Krone A, Reeve R M, Weigand M, Agrawal P, Lemesh I, Mawass M A, Fischer P, Kläui M and Beach G S D 2016 *Nat. Mater.* **15** 501
[26] Caretta L, Mann M, Büttner F, Ueda K, Pfau B, Günther C M, Hessing P, Churikova A, Klose C, Schneider M, Engel D, Marcus C, Bono D, Bagschik K, Eisebitt S and Beach G S D 2018 *Nat. Nanotechnol.* **13** 1154
[27] Büttner F, Lemesh I, Schneider M, Pfau B, Günther C M, Hessing P, Geilhufe J, Caretta L, Engel D, Krüger B, Viefhaus J, Eisebitt S and Beach G S D 2017 *Nat. Nanotechnol.* **12** 1040
[28] Woo S, Song K M, Zhang X, Zhou Y, Ezawa M, Liu X, Finizio S, Raabe J, Lee N J, Kim S I, Park S Y, Kim Y, Kim J Y, Lee D, Lee O, Choi J W, Min B C, Koo H C and Chang J 2018 *Nat. Commun.* **9** 959
[29] Yu G, Upadhyaya P, Li X, Li W, Kim S K, Fan Y, Wong K L, Tserkovnyak Y, Amiri P K and Wang K L 2016 *Nano Lett.* **16** 1981
[30] Yu X, Morikawa D, Tokunaga Y, Kubota M, Kurumaji T, Oike H, Nakamura M, Kagawa F, Taguchi Y, Arima T H, Kawasaki M and Tokura Y 2017 *Adv. Mater.* **29** 1606178
[31] White J S, Prša K, Huang P, Omrani A A, Živković I, Bartkowiak M, Berger H, Magrez A, Gavilano J L, Nagy G, Zang J and Rønnow H M 2014 *Phys. Rev. Lett.* **113** 107203
[32] Mochizuki M and Watanabe Y 2015 *Appl. Phys. Lett.* **107** 082409
[33] Hsu P J, Kubetzka A, Finco A, Romming N, von Bergmann K and Wiesendanger R 2017 *Nat. Nanotechnol.* **12** 123
[34] Schott M, Bernand-Mantel A, Ranno L, Pizzini S, Vogel J, Béa H, Baraduc C, Auffret S, Gaudin G and Givord D 2017 *Nano Lett.* **17** 3006
[35] Huang P, Cantoni M, Kruchkov A, Rajeswari J, Magrez A, Carbone F and Rønnow H M 2018 *Nano Lett.* **18** 5167
[36] Srivastava T, Schott M, Juge R, Křižáková V, Belmeguenai M, Roussigné Y, Bernand-Mantel A, Ranno L, Pizzini S, Chérif S M, Stashkevich A, Auffret S, Boulle O, Gaudin G, Chshiev M, Baraduc C and Béa H 2018 *Nano Lett.* **18** 4871
[37] Hu J M, Chen L Q and Nan C W 2016 *Adv. Mater.* **28** 15
[38] Sun Y, Ba Y, Chen A, *et al.* 2017 *ACS Appl. Mater. Interfaces* **9** 10855
[39] Hu J M, Yang T and Chen L Q 2018 *npj Comput. Mater.* **4** 62
[40] Ghidini M, Mansell R, Maccherozzi F, Moya X, Phillips L C, Yan W, Pesquera D, Barnes C H W, Cowburn R P, Hu J M, Dhesi S S and Mathur N D 2019 *Nat. Mater.* **18** 840
[41] Ma C, Zhang X, Xia J, Ezawa M, Jiang W, Ono T, Piramanayagam S N, Morisako A, Zhou Y and Liu X 2019 *Nano Lett.* **19** 353
[42] Xu X, Li X L, Semenov Y G and Kim K W 2019 *Phys. Rev. Applied* **11** 024051
[43] Wang Y, Wang L, Xia J, Lai Z, Tian G, Zhang X, Hou Z, Gao X, Mi W, Feng C, Zeng M, Zhou G, Yu G, Wu G, Zhou Y, Wang W, Zhang X X and Liu J 2020 *Nat. Commun.* **11** 3577
[44] Ba Y, Zhuang S, Zhang Y, Wang Y, Gao Y, Zhou H, Chen M, Sun W, Liu Q, Chai G, Ma J, Zhang Y, Tian H, Du H, Jiang W, Nan C, Hu J M and Zhao Y 2021 *Nat. Commun.* **12** 322
[45] Dumas R K, Gredig T, Li C P, Schuller I K and Liu K 2009 *Phys. Rev. B* **80** 014416
[46] Schneider M, Hoffmann H and Zweck J 2001 *Appl. Phys. Lett.* **79** 3113
[47] Donahue M J and Porter D G 1999 *National Institute of Standards and Technology*, Gaithersburg, MD
[48] Zhou H, Fan X, Wang F, Jiang C, Rao J, Zhao X, Gui Y S, Hu C M and Xue D 2014 *Appl. Phys. Lett.* **104** 102401
[49] Peng B, Zhou Z Y, Nan T X, Dong G H, Feng M M, Yang Q, Wang X J, Zhao S S, Xian D, Zhuang-De J, Ren W, Ye Z G, Sung N X and Liu M 2017 *ACS Nano* **11** 4337
[50] Baek S H, Park J, Kim D M, *et al.* 2011 *Science* **334** 958
[51] Bi C, Liu Y, Newhouse-Illige T, Xu M, Rosales M, Freeland J W, Mryasov O, Zhang S, te Velthuis S G E and Wang W G 2014 *Phys. Rev. Lett.* **113** 267202
[52] Bauer U, Yao L, Tan A J, Agrawal P, Emori S, Tuller H L, van Dijken S and Beach G S D 2015 *Nat. Mater.* **14** 174
[53] Fassatoui A, Garcia J P, Ranno L, Vogel J, Bernand-Mantel A, Béa H, Pizzini S and Pizzini S 2020 *Phys. Rev. Applied* **14** 064041
[54] Hou Z P, Wang Y D, Lan X M, *et al.* 2022 *Adv. Mater.* **34** 2107908